EFFECT OF DIFFERENT HEAT EXCHANGE TUBE SURFACE CHARACTERISTICS AND MICROSTRUCTURES ON HEAT TRANSFER PERFORMANCE.

Heng Li [a], Xiaojing Ma [a,b*], Jiamei Cao[a], Tusongjiang Kari[a], Lin Li[a], Yifang Meng[a]

[a] College of Electrical Engineering, Xinjiang University, Urumqi, P.R. China;

[b] Engineering Research Center of Northwest Energy Carbon Neutrality, Ministry of Education, Xinjiang University, Urumqi, P.R. China

*Corresponding author: Xiaojing Ma; E-mail: maxiaojing1983@xju.edu.cn

Falling film evaporation is an efficient phase-change heat transfer technology widely used in refrigeration and industrial applications. An experimental platform for horizontal tube falling film evaporation was designed and constructed. Experiments were conducted on smooth tubes, T-shaped finned tubes, and finned tubes. The results show that the heat transfer performance of finned tubes is not as good as that of smooth tubes when the spray density (Γ) is less than 0.048 kg·m⁻¹·s⁻¹. When the tube diameter decreases, the heat transfer performance of finned tubes exceeds that of smooth tubes at approximately Γ = 0.032 kg·m⁻¹·s⁻¹. However, the heat transfer performance of T-shaped finned tubes has consistently been superior to that of smooth tubes. After hydrophilic coating treatment, the heat transfer performance of T-shaped finned tubes and smooth tubes initially increased, then decreased, and eventually stabilized as spray density increased. At a saturation temperature (T_{sat}) of 70 °C and Γ = 0.0087 kg·m⁻¹·s⁻¹, the heat transfer coefficient decreases due to deterioration on the tube surface. Under identical experimental conditions, the heat transfer performance of the T-shaped finned tube and the finned tube improved by approximately 56%-62% and 28%-35%, respectively, compared with the smooth tube. Hydrophilically modified smooth, T-shaped finned, and finned tubes improved heat transfer coefficients by approximately 51%, 45%, and 11%, respectively. Overall, the T-shaped finned tube demonstrated superior performance compared to other tubes under all tested conditions, making it a promising choice for enhanced heat transfer applications.

Keywords: falling film evaporation; heat transfer coefficient; enhanced heat transfer; enhanced tube; surface wettability

1. Introduction

Falling film evaporation (FFE) is widely utilized in desalination, refrigeration, and the petrochemical industries as an efficient phase-change heat transfer (HT) method [1]. FFE is categorized into horizontal tube, vertical tube, and full liquid types. Horizontal tube FFE is prioritized for research due to its higher HT efficiency, simpler structure, and lower operational costs [2]. However, the HT mechanism of horizontal tube FFE is complex and influenced by factors such as

operating conditions, equipment design, and surface characteristics [3]. Operating conditions, including spray density and evaporation temperature, affect the thickness and disturbance of the liquid film, thus impacting heat transfer [4]. Equipment design, such as tube arrangement and spray header design, influences the uniformity and flow characteristics of the liquid film, determining overall HT efficiency [5]. Surface characteristics, such as hydrophilicity and material, affect liquid film formation and spreading, further influencing the HT coefficient [6].

Several studies have shown that increasing spray density can improve the overall HT coefficient, though the effect varies across studies [7,8]. Generally, the HT coefficient tends to increase with higher spray density. Xie et al. [9] observed improved HT performance at spray densities between 0.042 to 0.200 $kg \cdot m^{-1} s^{-1}$, due to increased film disturbance and stronger convection. Other studies suggest that the HT coefficient may plateau or decline at higher spray densities [10-12]. Ji et al. [13] found that the HT coefficient with R134a initially rose but plateaued with higher spray densities. Similarly, Jin et al. [14] and Zhao et al. [15] observed an initial rise followed by a slight decline in the HT coefficient as spray density increased. Thus, while increasing spray density generally improves the HT coefficient, the relationship varies depending on the experimental conditions and setups.

Moreover, research has explored the relationship between evaporation temperature and the HT coefficient [16,17]. Hsu et al. [18] found a strong positive correlation between evaporation temperature and HT efficiency, attributed to the effect of temperature on liquid properties, which enhances film turbulence. Furthermore, Current studies on finned tubes in horizontal FFE are limited, but existing research shows that finned tubes improve HT efficiency by increasing surface area, with performance influenced by fin structure, spray density, and spray header design [19,20]. Hydrophilic and superhydrophilic surfaces also boost HT performance, with superhydrophilic surfaces showing superior effectiveness at lower spray densities [21].

In conclusion, while the HT challenges in horizontal tube FFE have been well studied, debates continue regarding the HT characteristics of hydrophilic surfaces on enhanced tubes. The variability of the HT coefficient with changes in spray densities and evaporation temperatures in hydrophilic finned tubes remains a key issue. This study aims to experimentally assess HT performance under different conditions to determine which heat exchanger tubes provide optimal efficiency. The findings aim to provide insights to improve HT efficiency in the FFE process, as detailed in the upcoming experimental analysis.

2. Experimental installation

2.1. Experimental system

A horizontal tube FFE HT test platform was carefully designed and constructed. Figures 1(a) and 1(b) show the process flow and equipment layout. The system, detailed in Figure 1(a), consists of three circuits: working fluid, steam circulation, and cold glycol. Water circulates as the working fluid. Key components include an evaporation drum, circulation pump, and measurement instruments. The system operates by pumping the working fluid from the evaporator to the liquid distributor. The fluid flows over the test tube by gravity, where it is heated and evaporated by steam. The vapor condenses near the cooling tubes and recirculates back to the evaporator. Figure 2 illustrates the FFE process within the evaporator.

The steam circulation loop includes a vapor generator, reservoir, steam pump, and measuring device. Steam produced by the generator passes through the evaporator, condenser, reservoir, and measuring device, driven by the steam pump. After phase change in the evaporator, the gas enters a gas-liquid state, and after phase change in the condenser, it becomes liquid water. The liquid is pumped back to the generator, completing the steam cycle.

The cold glycol circuit consists of an air cooler, cold fluid tank, steam condensate pumps, and a measuring device. The system is divided into three loops: one cools steam from the evaporator, turning it into liquid water; the second maintains the working medium temperature; and the third ensures steam entering the storage tank is fully condensed into liquid.

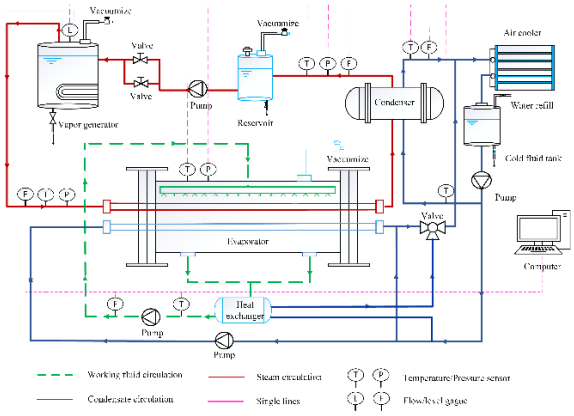

FIG. 1(a). Schematic diagram of the experiment system

FIG. 1(b). Experimental equipment

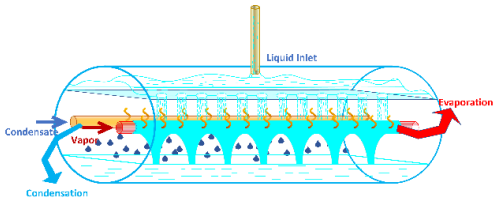

FIG. 2. Operating principle in the evaporator

2.2. Experimental Test Tubes

During the experiment, we selected T-shaped finned, ordinary finned, and smooth tubes for comparison. The dimensions of the T-shaped and ordinary finned tubes were designed to increase the HT area and enhance liquid film disturbance, improving the convective HT coefficient. These dimensions were based on previous studies [22][23], considering manufacturability and compatibility with the apparatus. Research shows that fin geometry (height and spacing) affects HT and fluid dynamics. For example, while increasing fin height expands the HT area, it also raises flow resistance, reducing overall efficiency. Thus, we balanced HT performance with liquid film flow characteristics to identify tubes better suited for FFE. Figures 3(a) and 3(b) show the tube structures and dimensions.

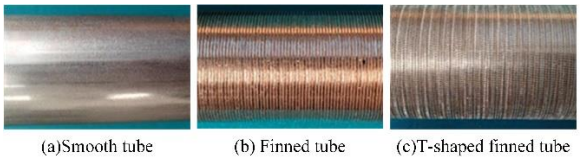

FIG. 3(a). Heat exchange tube

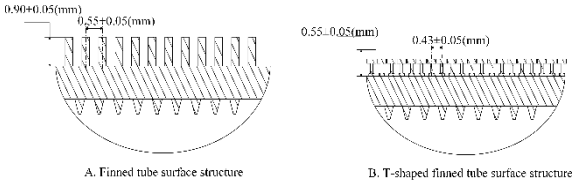

FIG. 3(b). Heat exchange tube structure

Tab. 1. Heat exchange specifications

Type of heat transfer tube	*L*/㎜	*δ*/㎜	*e*/㎜	*fpi*
Smooth	**2000**	**1**	**-**	**-**
Finned tube	**2000**	**1**	**0.9**	**58**
T-shaped finned tube	**2000**	**1**	**0.55**	**60**

3. Data Processing and Analysis

3.1. Data Formula Derivation

To minimize errors in heat balance calculations, the experiment focuses on steam inside the tube. Initially, heat exchange with the external liquid film cools the vapor to a gas-liquid mixture. Subsequent heat exchange with glycol in the condenser fully condenses the vapor into liquid. A liquid-viewing mirror monitors the phase transition, verifying that the two-phase flow transitions completely to liquid, ensuring the accuracy of results. The experiment strictly adheres to the principle of energy conservation, as expressed by the following equation:

$$Q_e = Q_i - Q_c + Q_s \tag{1}$$

Where Q_e represents the heat exchanged in the FFE section of the heat exchange tube.; Q_s is the heat loss in the pipe, which is negligible compared to the total heat transfer due to the insulation used and the short length of the tube. Q_i is the total heat transferred within the heat exchange tube; Q_c is the heat exchanged between the heat exchange tube and the condenser. Furthermore, Q_i satisfies the following relational equation:

$$Q_i = F_v \cdot \rho_v \cdot (H_v - H_l) \tag{2}$$

Where F_v is the imported steam's flow rate; ρ_v is the steam's density; H_v is the saturated vapor enthalpy corresponding to the temperature of the imported steam and H_l is the saturated water enthalpy corresponding to the temperature of the imported steam.

Q_c satisfies the following relation：

$$Q_c = G_{MEG} \cdot \rho_{MEG} \cdot C_p \cdot (T_{c,in} - T_{c,out}) \tag{3}$$

Where G_{MEG} represents the ethylene glycol's flow rate; ρ_{MEG} is the ethylene glycol's density; C_p denotes the specific heat capacity of the ethylene glycol, calculated at the average temperature $(T_{C,in}+T_{C,out})/2$, $T_{C,in}$ is the temperature at the condenser's inlet and $T_{C,out}$ is the temperature at the condenser's outlet.

To compute the overall HT coefficient *K*, we can use the formula [24]:

$$K = \frac{Q_e}{A_{out} \cdot \Delta T_{LMTED}} \tag{4}$$

Where A_{out} represents the external surface area of the tube. The logarithmic mean temperature difference, ΔT_{LMTED} is defined by the equation [24]:

$$\Delta T_{MTED} = \frac{T_{e,in} - T_{e,out}}{\ln\left(\frac{T_{e,in} - T_{sat}}{T_{e,out} - T_{sat}}\right)} \tag{5}$$

Where T_{sat} is the evaporation temperature; $T_{e,in}$ is the water temperature at the inlet of the evaporation tube and $T_{e,out}$ the water temperature at the outlet of the condenser in the evaporation tube.

The Reynolds number, a critical parameter in the FFE process, is calculated using the equation [25]:

$$\mathrm{Re} = \frac{4\Gamma}{\mu} \tag{6}$$

Where Γ is the spray density for FFE and μ is the viscosity coefficient of the working material.

The magnitude of the spray density represents the magnitude of the work mass flow rate, and the spray density in this study refers to the one-way spray density that satisfies the following correlation equation [25]:

$$\Gamma = \frac{G}{2 \times L \times 3600} \tag{7}$$

Where G represents the work mass flow rate and L denotes the length over which the spray is distributed.

3.2. Uncertainty and Error Analysis

In experimental research, to ensure the experimental data is closer to the actual value, a measuring instrument with higher precision should be selected. However, discrepancies between experimental data and true values are unavoidable. Consequently, it's vital to examine the origins and extents of these experimental errors to assess the trustworthiness of the data collected. Usually, the error comes from the accuracy of the equipment and the uncertainty transmission of the calculation process.

Usually, the error comes from the accuracy of the equipment and the uncertainty transmission of the calculation process. As some of the parameters are measured directly by the meter, the error comes from the accuracy of the meter itself, as shown in Table 2. And for those parameters that cannot obtained by direct measurement, calculations are necessary to get them. Due to the propagation of uncertainty through the calculation process, this parameter is derived using the error analysis method outlined by Kline [26]. The findings are presented in Table 3, indicating that the uncertainty in the HT coefficient is below 6%.

Based on reference [27], for similar falling film HT experiments, an uncertainty in the HT coefficient of less than 10% is generally considered acceptable. Therefore, the 6% uncertainty in this experiment fully meets the experimental requirements and does not significantly affect the accuracy of the final results. Additionally, through repeated experiments and optimization of the experimental design, we further reduced random errors, thereby enhancing the reliability of the data.

Table 2. Experimental test errors

Measuring device	Error
Pressure transmitters	±0.25%
thermocouple	±0.05℃
Electromagnetic flowmeter	±0.5%
Liquid level sensors	±0.5%

Table 3. Uncertainty analysis

Experimental parameters	Uncertainty
HT temperature difference	2.5%
Spray length	0.5%
Spray density	0.5%
HT coefficient	5.6%

4. Experimental Results and Discussion

The tested parameters included a spray density of 0.0083 to 0.1 kg·m^{-1}s^{-1}, an evaporation temperature of 50 to 70°C, and an inlet steam temperature of 60 to 90°C. Data was recorded every 30 seconds over 20 minutes once conditions stabilized. Seven sets of experiments were conducted under the same conditions, and the average of these sets was used to ensure accuracy and minimize experimental variability.

4.1. Effect of tube diameter and spray density on the heat transfer coefficient of different heat exchange tubes

Figure 4 illustrates the overall HT coefficient, K, as a function of spray density and tube diameter at a fixed Δt=10°C and T_{sat}=65°C.

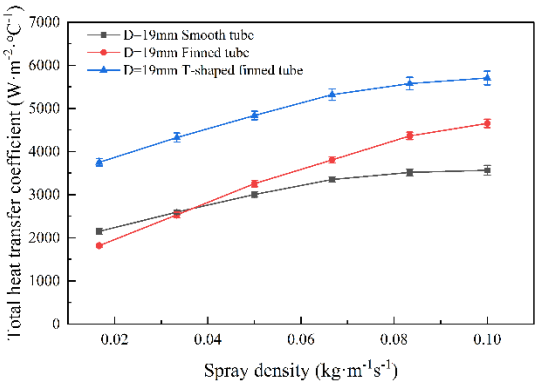

FIG. 4(a). Variation rule of total HT coefficient with spray density when D=19mm

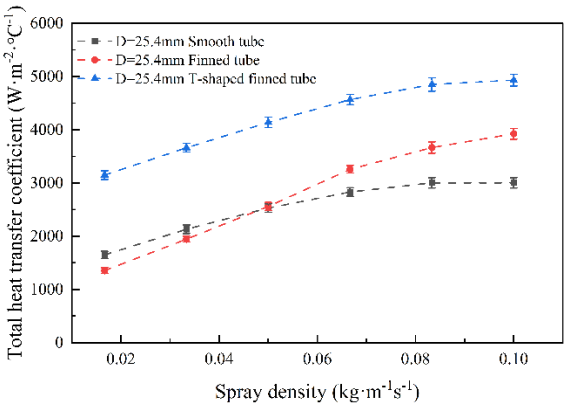

FIG. 4(b). Variation rule of total HT coefficient with spray density when D=25.4mm

Fig. 4. Variation rule of total HT coefficient with spray density and tube diameter

The graph shows that decreasing tube diameter and increasing spray density both enhance the HT coefficient. This is due to three factors: first, when the tube diameter decreases, the increased spray spacing allows the liquid film to accelerate more before droplet impact, enhancing droplet velocity and increasing the film's turbulent kinetic energy. Second, a smaller diameter reduces the

distance the liquid film flows over the heat exchanger tube, lessening the deceleration from viscous forces. Third, higher spray density increases both the HT area and the liquid film's inertia and fluctuation. However, as the film thickens, the thermal boundary layer also thickens, gradually slowing the increase in HT coefficient.

Notably, at low spray densities, the HT performance of finned tubes is lower than that of smooth tubes. This is primarily due to the excessive fin height, which hinders the lateral spreading of the liquid film, negatively impacting HT. The taller fins create more resistance for the liquid film to spread evenly, leading to poorer HT. Reducing the tube diameter can partially alleviate this issue, as it shortens the distance the liquid film needs to travel. In contrast, T-shaped finned tubes improve lateral diffusion of the liquid film due to their lower fin height. The T-shaped design prevents liquid droplets from falling directly into the grooves, creating a buffer zone that promotes more even liquid distribution. As a result, the HT capacity of T-shaped finned tubes is significantly better than that of smooth tubes.

4.2. Effect of evaporating temperature on heat transfer coefficients of different heat exchanger tubes

Figure 5 shows the variation in the overall HT coefficient, K, with evaporation temperatures from 50 to 70°C, at a sprinkling density of 0.083 kg·m^{-1}·s^{-1}, Δt=10°C, and tube diameter of 25.4 mm.

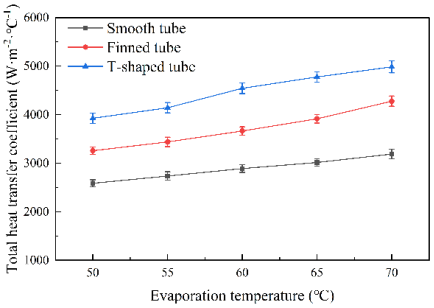

Fig. 5. Variation rule of total HT coefficient with evaporation temperature.

The results indicate that as the evaporation temperature increases, the total HT coefficient rises. This is due to the decrease in water's surface tension and viscosity at higher temperatures, which enhances water turbulence and thins the laminar flow layer outside the tube, strengthening convective HT. Notably, finned and T-shaped finned tubes show a greater increase in HT coefficient compared to smooth tubes, attributed to surface treatments that intensify turbulence as evaporation temperature rises, accelerating the HT coefficient's growth.

4.3. influence of tube surface wettability on the total heat transfer coefficient

4.3.1 Hydrophilic surface preparation

Currently, the primary methods for preparing hydrophilic surfaces include electrochemical deposition, sol-gel self-assembly, and photochemical catalysis [28]. To enhance the hydrophilicity of the heat exchange tube, a detailed coating procedure was used. After thoroughly cleaning the tube, a nano-coating was applied, followed by a hydrophilic spray coating after 2-3 hours of setting. This significantly improved surface wettability, as

shown in Figure 6. The contact angle on the smooth tube decreased from 82° to 31°, indicating a marked increase in hydrophilicity. However, due to the microstructure of the finned and T-shaped finned tubes, quantitative contact angle analysis could not be performed on these tubes.

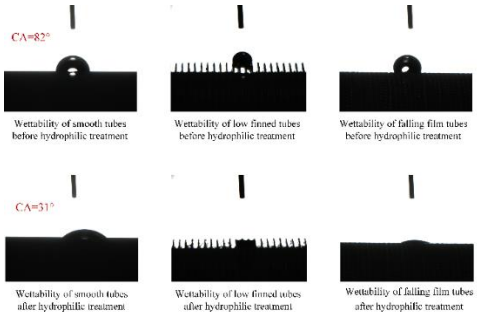

Fig. 6. Wettability comparison of tube surfaces

4.3.2 The spray effect of the hydrophilic surface

The spreading behaviors of liquid films on different tube types—namely, a smooth tube treated with a hydrophilic coating, a finned tube, and a T-shaped finned tube—were investigated across various Reynolds numbers (*Re*). Comparative experimental findings are presented in Figures. 7(a), 7(b), 7(c), 7(d), 7(e) and 7(f), illustrating the distinct liquid film dynamics on each tube type.

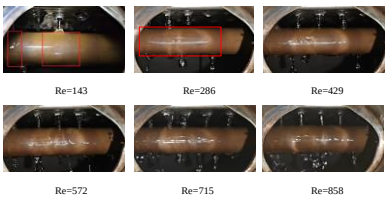

FIG. 7(a). Wetting of smooth tube surface before hydrophilic treatment

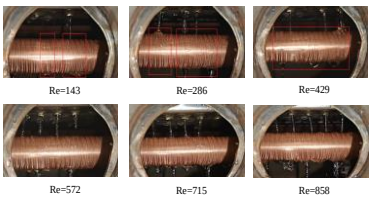

FIG. 7(b). Wetting of T-shaped finned tube surface before hydrophilic treatment

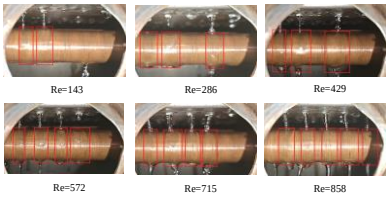

FIG. 7(c). Wetting of finned tube surface before hydrophilic treatment

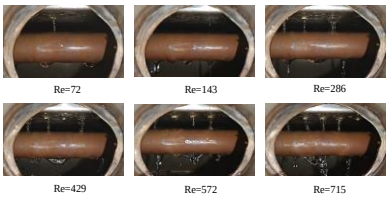

FIG. 7(d). Wetting of smooth tube surface after hydrophilic treatment

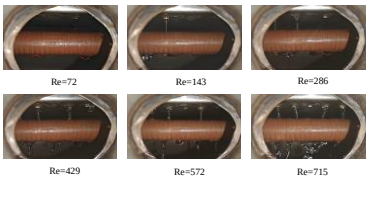

FIG. 7(e). Wetting of T-shaped finned tube surface after hydrophilic treatment

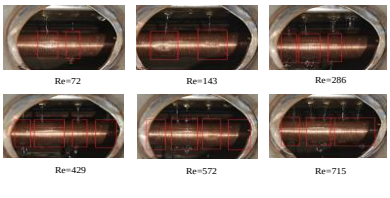

FIG. 7(f). Wetting of finned tube surface after hydrophilic treatment

As can be seen from the spray effect diagram, the hydrophilic T-shaped finned tubes and light tubes are completely wetted at *Re* = 72, while the same spray effect is achieved only at *Re*=286 compared to the untreated surface. At identical Reynolds numbers, the hydrophilic treatment on the finned tube marginally enhances the surface wetting area. This is mainly due to the fact that after hydrophilic treatment, the contact angle on the surface of the heat transfer tube is reduced, resulting in a larger spreading area for the liquid film. However, due to the high fin height of the finned tube, and

the liquid droplets do not have a lateral cushion after dropping as in the case of the T-shaped finned tube. Therefore, the spreading area of the liquid film is not greatly improved for finned tubes.

4.3.3 The influence of the hydrophilic surface of different heat transfer tubes on the heat transfer performance

Figures 8 and 9 show the effects of evaporation temperature and spray density on the HT efficiency of smooth and T-shaped finned tubes. Increasing the evaporation temperature to 65°C improves HT performance for both tube types. However, at T_{sat}=70°C and Γ=0.0083 kg·m^{-1}·s^{-1}, elevated surface temperatures and reduced liquid film thickness accelerate evaporation, leading to deteriorating HT conditions and reduced overall efficiency. Both tubes have a diameter of 25.4 mm. The HT deterioration is more severe in T-shaped finned tubes compared to smooth tubes. This is because some liquid penetrates the grooves of the T-fin upon impact, while other droplets, due to the buffer design, maintain lateral spreading speed and continue to penetrate the grooves. Although the HT coefficient inside the grooves is higher due to fin dissipation, the liquid film evaporates faster, worsening HT deterioration.

Figure 10 examines the impact of various parameters on the HT performance of finned tubes, showing consistent improvement with increasing evaporation temperatures. This trend is similar to uncoated finned tubes but with slight enhancements at the same spray densities, due to improved longitudinal liquid film spread, though transverse spreading remains limited by the fins' obstruction.

As seen in Figures 8 and 9, the HT performance of T-shaped finned and smooth tubes initially rises, then falls, and finally stabilizes with increasing spray density. This differs from pre-hydrophilic treatment behavior. The enhanced wettability of hydrophilic-treated tubes promotes better liquid film spreading at lower spray densities. At Γ=0.025 kg·m^{-1}·s^{-1}, the surface is fully wetted, the liquid film thins, and HT efficiency peaks. However, as spray density further increases, the liquid film thickens, raising thermal resistance and reducing the overall HT coefficient. At Γ=0.058 kg·m^{-1}·s^{-1}, the impact on HT diminishes, stabilizing the HT coefficient.

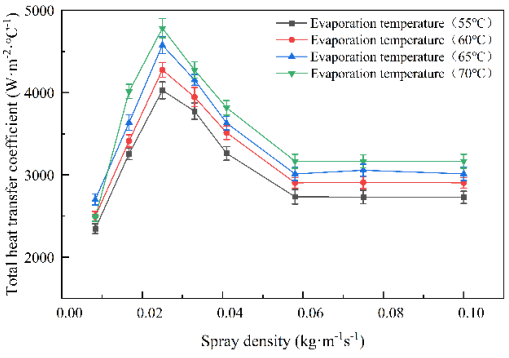

FIG. 8. Effect of evaporation temperature and spray density on HT performance of smooth tube

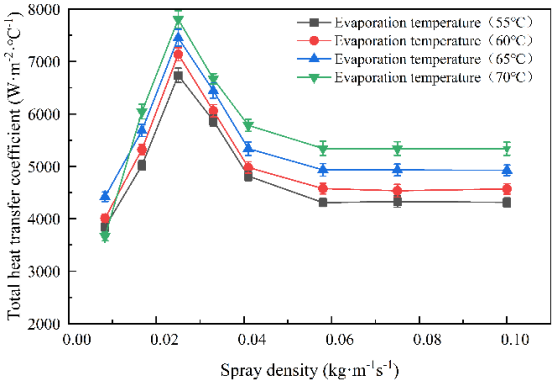

FIG. 9. Effect of evaporation temperature and spray density on HT performance of T-shaped finned tube

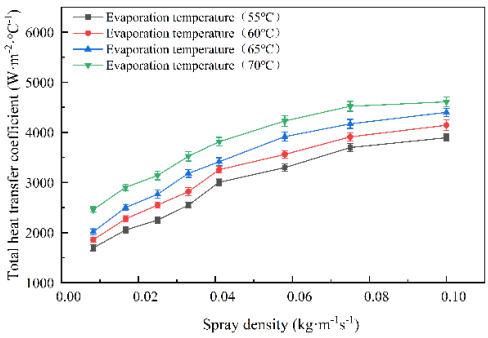

FIG. 10. Effect of evaporation temperature and spray density on HT performance of finned tube

The analysis shows that hydrophilic treatment significantly improves the HT performance of various tubes. To quantify this, we compared the HT coefficients before and after treatment and calculated the improvement rates. The rate was determined by comparing the maximum HT coefficient after treatment with the final stabilized value and calculating the percentage difference. Results show improvements of 51%, 11%, and 45% for T-shaped finned, finned, and smooth tubes, respectively. Additionally, by comparing the maximum HT coefficients under fixed conditions (see Figures 4, 5, 8, 9, and 10), improvement rates were expressed as ranges: 56%-62% for T-shaped finned tubes and 28%-35% for finned tubes. This range-based approach better captures the effects of varying operating conditions on HT performance.

5. Conclusion

This study presents the design and construction of a horizontal tube FFE HT test platform. The HT efficiency of smooth, T-shaped finned, and finned tubes was experimentally investigated. The research outlines HT performance trends for different tubes under varying spray densities, evaporation temperatures, and surface wettability. Key findings include:

(1) An increase in spray density and a decrease in tube diameter improved HT performance for all three tube types. Finned tubes showed better HT performance with higher spray densities, while smooth and T-shaped finned tubes exhibited an initial increase followed by a plateau. At low spray densities, finned tubes performed worse at high temperatures compared to smooth tubes, but this could be improved by adjusting the tube diameter.

(2) Raising the evaporation temperature enhanced the HT performance for all three tube types. However, compared to smooth tubes, the T-shaped finned and finned tubes benefited the most from increased evaporation temperatures.

(3) Hydrophilic treatment significantly improved HT performance: 51% for T-shaped finned tubes, 45% for smooth tubes, and 11% for finned tubes. Both T-shaped finned and smooth tubes showed an initial increase in HT performance with higher spray densities, followed by a decline and stabilization. An increase in evaporation temperature below 70°C also enhanced HT performance, but at T_{sat}=70°C and Γ=0.0087 kg·m^{-1}·s^{-1}, a decline was observed for both tubes, with more severe deterioration in T-shaped finned tubes. The HT performance of finned tubes remained unchanged compared to pre-treatment levels under the same conditions.

(4) Comparatively, the T-shaped finned tube's performance improved by approximately 56-62% relative to the smooth tube, and the finned tube exhibited 28-35% improvement over the smooth tube

under the same operational conditions. Therefore, the lower fin height and T-fin design are more favorable to improve the HT performance of FFE.

Acknowledgment

This work is supported by Xinjiang Uygur Autonomous Region Tianshan Talent Training Program(2022TSYCCX0054), Natural Science Foundation of Xinjiang Uygur Autonomous Region (2022D01C47)， Key Research and Development Task Special Project of Xinjiang Uygur Autonomous Region (2022B03028-5), National Natural Science Foundation of China (12362021).

Nomenclature

A	-area, [m^2]	Δ	-variable differential, [-]
D	-outer diameter of tube, [mm]	ρ	-density, $kg \cdot m^{-3}$
fpi	-external fins per inch, [-]		Subscript
e	-external fins height, [mm]	c	-condensation, [-]
G	-mass flow, [$kg \cdot h^{-1}$]	e	-evaporation, [-]
H	-enthalpy, [$kJ \cdot kg^{-1}$]	in	-inlet, [-]
K	-the total heat transfer efficient, [$W \cdot m^{-2} \cdot ℃^{-1}$]	l	-liquid, [-]
L	-length of test tube, [mm]	v	-vapor, [-]
Q	-heat exchange rate, [W]	$LMTD$	-logarithmic mean temperature difference, [-]
Re	-Reynolds number, [-]	MEG	-ethylene glycol, [-]
T	-temperature, [℃]	out	-outlet, [-]
C_p	-specific heat capacity, [$J \cdot kg^{-1} \cdot K^{-1}$]	sat	-saturation, [-]
Creek symbols		i	-inside of tube, [-]
Γ	-spraying density, [$kg \cdot m^{-1} \cdot s^{-1}$]		

References

[1]Ribatski, G., Jacobi, A. M., Falling-film evaporation on horizontal tubes—a critical review, *International journal of refrigeration.*, 28(2005),5, pp. 635-653

[2]Wang, J. K., et al., Simulation of falling film evaporation heat transfer in horizontal tubes based on optimized bionic structure, *Science Technology and Engineering.*, 23(2023),2, pp. 0580-09

[3]Dai, Z., et al., Falling-film heat exchangers used in desalination systems: A review, *International Journal of Heat and Mass Transfer.*, 185(2021),0017-9310, pp. 122407

[4]Chen, H., and Jebson R. S., Factors affecting heat transfer in falling film evaporators. *Food and Bioproducts Processing.*, 75(1997),2, pp. 111-116

[5]Abraham, R., and Mani, A., Heat transfer characteristics in horizontal tube bundles for falling film evaporation in multi-effect desalination system." *Desalination.*, 375 (2015), pp. 129-137

[6]Christmann, J.B., et al., Falling film evaporation with polymeric heat transfer surfaces. *Desalination.*, 308 (2013), pp.56-62

[7]Li, Q., et al., Experimental study of heat transfer performance of horizontal-tube falling film evaporator, *Desalination and Water Treatment.*, 218(2021),1944-3994, pp. 87-96

[8]Arshi, B. P., and Sudharsan, N. M. Experimental heat and mass transfer studies on horizontal falling film absorber using water-lithium bromide. *Thermal Science.*, 24(2020), 3 Part B, pp. 1923-1934

[9]Xie, L. X., et al., Study on heat-transfer performance of horizontal tube falling film evaporator, Chem. *CIESC Journal.*, 33(2014),11, pp. 2878

[10]Xu, B., et al., Numerical Study on Flow Heat Transfer Characteristics of Horizontal Tube Falling-Film Evaporator, *Journal of Thermal Science.*, 30(2021),4, pp. 1302-1317

[11]Chen, Z. G., et al., Numerical simulation and experimental study on heat transfer performance of falling film outside the horizontal tube, *Chemical Engineering & Machinery.*, 45(2018),6, pp. 757-763

[12]Chen, X., et al., Heat transfer of falling-film evaporation outside horizontal tube, *Acta Energiae Solaris Sinica.*, 36(2015),8, pp. 1996-2001

[13]Ji, W. T., et al., Falling film evaporation and nucleate pool boiling heat transfer of R134a on the same enhanced tube, *Applied thermal engineering.*,147(2019),1539-4311, pp. 113-121

[14]Jin, P. H., et al., Experimental investigation of R410A and R32 falling film evaporation on horizontal enhanced tubes, *Applied thermal engineering.*, 37(2018), 1539-4311, pp. 739-748

[15]Zhao, C. Y., et al., Experimental investigations of R134a and R123 falling film evaporation on enhanced horizontal tubes, *International journal of refrigeration.*, 75(2017),0140-7007, pp. 190-203

[16]Jin, P. H. et al., Heat transfer correlations of refrigerant falling film evaporation on a single horizontal smooth tube, *International Journal of Heat and Mass Transfer.*, 133(2019), 017-9310, pp. 96-106

[17]Zhao, C. Y., et al., Heat transfer correlation of the falling film evaporation on a single horizontal smooth tube, *Applied thermal engineering.*,103(2016), 1359-4311, pp. 177-186,

[18]Hsu, C. Y., et al., Experimental study of falling film evaporation of refrigerants, R32, R1234yf, R410A, R452B and R454B on horizontal tubes, *International Journal of Heat and Mass Transfer.*, 205(2023), 0017-9310, pp. 123914

[19]Cao, C.P., et al. Numerical study on the flow and heat-transfer characteristics of horizontal finned-tube falling-film evaporation: Effects of liquid column spacing and wettability. *International Journal of Heat and Mass Transfer.*, 188 (2022), pp. 122665

[20]Chen, J.D., Falling film mode transitions on horizontal enhanced tubes with two-dimensional integral fins: Effect of tube spacing and fin structures. *Experimental Thermal and Fluid Science.*, 101 (2019), pp. 241-250

[21]Zheng, Y. et al., Experimental study of falling film evaporation heat transfer on superhydrophilic horizontal-tubes at low spray density, *Applied Thermal Engineering.*, 111(2017), 1359-4311, pp. 1548-1556

[22]Liu H., et al. Experimental investigation of falling film evaporation on horizontal tubes at low-pressure. *Advanced Materials Research.*, 236(2011), pp. 1572-1575

[23]Li W., et al. Falling water film evaporation on newly-designed enhanced tube bundles. *International journal of heat and mass transfer.,* 54(2011), 13-14, pp. 2990-2997

[24]Tao, W. Q., Heat Transfer, 5th ed., *Higher Education Press*, Beijing, China, 2020, pp. 459-461.

[25]Wang Y.Z., et al. Experimental study on the scaling law of the heat exchange tube surface in the process of low-temperature single-effect distillation of high-mineralized mine water *Desalination and Water Treatment.*, 319(2024), pp. 100571

[26]Kline, S. J., The purposes of uncertainty analysis, Journal of Fluids Engineering,107/153(1985)

[27]Liu S.L., et al. Experimental study on the distribution of local heat transfer coefficient of falling film heat transfer outside horizontal tube. *International Journal of Heat and Mass Transfer.,* 170(2021), pp. 121031

[28]Ahmad, D., et al., Hydrophilic and hydrophobic materials and their applications, *Part A: Recovery, Utilization, and Environmental Effects.*, 40(2018), 22, pp. 2686–2725

Submitted: 28.07.2024.

Revised: 24.10.2024.

Accepted: 27.10.2024